
Measurements of the Ca II infrared triplet emission lines of pre-main-sequence stars

¹Mai Yamashita, ¹Yoichi Itoh, ²Yuhei Takagi

¹Nishi-Harima Astronomical Observatory, Center for Astronomy, University of Hyogo, 407-2
Nishigaichi, Sayo, Sayo, Hyogo 679-5313

²Subaru Telescope, National Astronomical Observatory of Japan, 650 North A'ohoku Place,
Hilo, HI 96720, U.S.A.

*E-mail: yamashita@nhao.jp

Received (2020 March 19); Accepted (2020 July 3)

Abstract

We investigated the chromospheric activity of 60 pre-main-sequence (PMS) stars in four molecular clouds and five moving groups. It is considered that strong chromospheric activity is driven by the dynamo processes generated by the stellar rotation. In contrast, several researchers have pointed out that the chromospheres of PMS stars are activated by mass accretion from their protoplanetary disks. In this study, the Ca II infrared triplet (IRT) emission lines were investigated utilizing medium- and high-resolution spectroscopy. The observations were conducted with Nayuta/MALLS and Subaru/HDS. Additionally, archive data obtained by Keck/HIRES, VLT/UVES, and VLT/X-Shooter was used. The small ratios of the equivalent widths indicate that Ca II IRT emission lines arise primarily in dense chromospheric regions. Seven PMS stars show broad emission lines. Among them, four PMS stars have more than one order of magnitude brighter emission line fluxes compared to the low-mass stars in young open clusters. The four PMS stars have a high mass accretion rate, which indicates that the broad and strong emission results from a large mass accretion. However, most PMS stars exhibit narrow emission lines. No significant correlation was found between the accretion rate and flux of the emission line. The ratios of the surface flux of the Ca II IRT lines to the stellar bolometric luminosity, R'_{IRT} , of the PMS stars with narrow emission lines are as large as the largest R'_{IRT} of the low-mass stars in the young open clusters. This result indicates that

most PMS stars, even in the classical T Tauri star stage, have chromospheric activity similar to zero-age main-sequence stars.

Key words: stars: pre-main sequence — stars: chromospheres — stars: activity — techniques: spectroscopic

1 Introduction

Chromosphere is the region between the photosphere and corona. The temperature of the chromosphere gradually increases with radial distance to the photosphere, in case of the Sun, it is from almost 4000 K at the bottom to 8000 K at the top (Vernazza et al. 1981). Because of these high temperature, atoms emit some permitted lines like $H\alpha$ and Ca II. Several high spatial-resolution observations of the Sun show that in the chromosphere the above mentioned emission lines form under the influence of strong magnetic fields, such as faculae and plages near dark spots (Linsky 2017). The Hinode satellite has obtained space- and time-resolved images of the solar chromosphere and revealed its energetic activity (Katsukawa et al. 2007). Over a 30 year period, Livingston (2007) showed that fluxes of the Ca II K, $H\alpha$, and He I lines were strong when the solar magnetic activity was high. These observations revealed the relationship between the emission line strengths and the chromospheric activity induced by the magnetic field.

For main-sequence stars, chromospheric activity is often discussed in relation to stellar rotation. It is claimed that chromospheric activity is driven by the magnetic field, which is generated by the dynamo process. Wilson (1978) showed that chromospheric activity analogous to that associated with the solar magnetic activity cycle is ubiquitous in stars along the lower main-sequence stars. As mentioned in Noyes et al. (1984), rotation is not the only parameter related to the dynamo process, the stellar mass, spectral type, depth of convection zone, and convective turnover time (τ_c) are also related to the process. These five parameters are included in the Rossby number (N_R), which is defined as P_{obs}/τ_c , where P_{obs} is the stellar rotational period. According to standard dynamo theory in Parker (1955), the magnetic activity at the stellar surface is getting stronger with increasing rotation speed and strength of differential rotation.

It is well established that a young stars are fast rotators (e.g. Bouvier et al. 1990). Skumanich et al. (1972) found that the luminosity of the Ca II emission lines and the rotational velocity of solar-mass stars with an age of 10^7 yr are one order of magnitude larger than those of stars with 10^{10} yr. Soderblom et al. (1993) revealed strong emission lines of the Ca II infrared triplet (IRT ;

$\lambda 8498, 8542, 8662 \text{ \AA}$) of low-mass stars in a young open cluster, M45 (age $130 \pm 20 \text{ Myr}$, $0.6 - 1.4 M_{\odot}$). Marsden, Carter, & Donati (2009) observed low-mass stars in young open clusters, IC 2391 and IC 2602, including rapidly rotating stars. The age of IC 2391 and IC 2602 is $50 \pm 5 \text{ Myr}$ and $30 \pm 5 \text{ Myr}$, respectively (Stauffer et al. 1997 ; Navascues et al. 2004). The cluster members are considered to be on the zero-age main-sequence (ZAMS) or in the last phase of evolving to ZAMS with a mass between $0.8 M_{\odot}$ and $1.5 M_{\odot}$. Soderblom et al. (1993) and Marsden, Carter, & Donati (2009) calculated R'_{IRT} from the equivalent widths (EQWs). R'_{IRT} describes the ratio of the surface flux of the Ca II IRT emission lines to the stellar bolometric luminosity. They found that R'_{IRT} is constant at levels of around $\log R'_{\lambda 8498} \sim -4.4$, $\log R'_{\lambda 8542} \sim -4.2$, and $\log R'_{\lambda 8662} \sim -4.3$ for stars with $\log N_{\text{R}} \leq -1.1$. These regions are called the saturated regime. For stars with $\log N_{\text{R}} \geq -1.1$, R'_{IRT} decreases with increasing N_{R} . This region is called the unsaturated regime. Marsden, Carter, & Donati (2009) suggested that the chromosphere is completely filled by the emitting region for stars in the saturated regime.

The idea that the activity of the chromospheres is driven by the dynamo process is widely accepted not only for low-mass main-sequence stars but also for pre-main-sequence (PMS) stars. However several previous studies showed that a certain portion of T Tauri stars (TTs) are slow rotators. Vogel and Kuhl (1981) found that low-mass PMS stars ($\leq 1.5 M_{\odot}$) generally rotate at less than $25 \text{ km} \cdot \text{s}^{-1}$. White & Basri (2003) revealed that all of the low-mass TTs in the Taurus-Auriga star forming region are slowly rotating ($v \sin i < 30 \text{ km} \cdot \text{s}^{-1}$). Hartmann et al. (1986) confirmed and extended the findings of Vogel and Kuhl (1981); they found that about 30% of the $0.5 - 1.0 M_{\odot}$ TTs in Taurus have rotational velocities at or below $10 \text{ km} \cdot \text{s}^{-1}$, and half have $v \sin i$ values between 10 and $15 \text{ km} \cdot \text{s}^{-1}$. However, previous studies also showed that a fraction of TTs exhibit strong Ca II emission lines (Hartmann, Soderblom & Stauffer 1986). Batalha & Basri (1993) constructed models of photosphere and chromosphere to fit the observed profiles of the Ca II IRT emission line for TTs with low accretion rates but null veiling. Those deep chromosphere models explain the emission characteristics of TTs, showing a narrow emission profile over a broad absorption feature (Calvet, Basri, & Kuhl 1984; Batalha et al. 1996). Calvet & Gullbring (1998) found that shock heating of the photosphere by emission of chromosphere result in a temperature inversion and the temperature increases in the chromosphere, as shown by deep chromospheric models. In contrast, Moto'oka & Itoh (2012) found no clear correlation between the EQWs of the Ca II IRT emission lines and stellar rotation velocity. As mentioned above, the rotation velocity is not the only parameter expected to be related to the dynamo process. The effective temperature (T_{eff}), τ_{c} , and the spectral distribution of the continuum flux change as PMS stars evolve.

Another indicator for chromospheric activity of PMS stars is mass accretion from their pro-

toplanetary disks. Moto’oka & Itoh (2012) found that the EQWs of the Ca II IRT emission lines decrease with stellar evolution from classical TTSs (CTTSs), transitional disk objects, weak-line TTSs (WTTSs), to ZAMS stars. They also revealed that PMS stars with high mass accretion rates have strong Ca II emission lines. Mohanty, Jayawardhana, & Basri (2005) investigated the chromospheric activity of CTTSs, very low-mass young stars ($0.075 \leq M_* < 0.15 M_\odot$), and young brown dwarfs ($M_* \leq 0.075 M_\odot$). The surface flux of the Ca II emission line at $\lambda 8662 \text{ \AA}$, $F'_{\lambda 8662}$, exhibit correlation with the associated mass accretion rate, \dot{M} , for approximately 4 orders of magnitude. Hence, Mohanty, Jayawardhana, & Basri (2005) claimed that the Ca II emission line is an excellent quantitative measure for the accretion rate. Hamann & Persson (1992a) carried out optical spectroscopy for 53 TTSs and 32 Herbig Ae/Be stars. They interpreted narrow emission lines such as Ca II and Mg I generated in the stellar chromosphere. The Ca II IRT emission lines of several TTSs and Herbig Ae/Be stars also have a broad line component. This profile can be well explained by the magnetospheric accretion model (e.g. Muzerolle et al. 1998).

In this study, we investigate the Ca II IRT emission lines of 60 PMS stars with medium- and high-resolution spectral data. We compare the rotation-activity relationship of the PMS stars with that of low-mass stars in young open clusters. The chromospheric activity of the cluster members is considered to be induced by dynamo activity. In the next section, we describe the observation and the data reduction procedures. In Section 3, we present the results, and in Section 4, we discuss the origin of the Ca II IRT emission lines and the emitting region on the stellar surface.

2 Observations and Data Reduction

1 Stellar parameters

All targets investigated in this study are listed in Table 1. These 60 objects are associated with four molecular clouds or five moving groups; the Taurus-Auriga molecular cloud, the Orionis OB 1c association, the Upper Scorpius association, the Perseus molecular cloud, the TW Hydrae association, the η Chamaeleontis cluster, the ”Cha-Near” region, the β Pictoris moving group, and the AB Doradus moving group. Hereafter, objects belonging to both molecular clouds and moving groups are called ”low-mass PMS stars”. We did not observe binaries or triplets listed in Ghez et al. (1993), Kraus et al. (2009), Kraus et al. (2012), Neuhauser et al. (1995), Leinert et al. (1993), Wahhaj et al. (2010) and Zuckerman & Song (2004).

Figure 1 presents the HR diagram of the investigated PMS stars. The filled circle symbols indicate PMS stars in molecular clouds. The open circles represent PMS stars in the moving groups. The luminosity, T_{eff} , and distance of the objects were taken from *Gaia* DR2 (Bailer-Jones et al.

2018). For objects, whose T_{eff} is not listed in *Gaia* DR2 (Bailer-Jones et al. 2018), we referred to other sources: Palla & Stahler (2002) for AA Tau, Kenyon & Hartmann (1995) for GH Tau, and Pecaut & Mamajek (2013) for HD 197481, RECX 09, and TWA 22. The solid lines indicate Canuto & Mazzitelli [CM] Alexander evolutionary tracks (D’Antona & Mazzitelli 1994). The stellar masses, M_* , masses of the bottom of the convective zone, M_{conv} , and ages of the target stars were estimated from their evolutionary tracks. For example, objects with $M_{\text{conv}} = 0 M_{\odot}$ are fully convective.

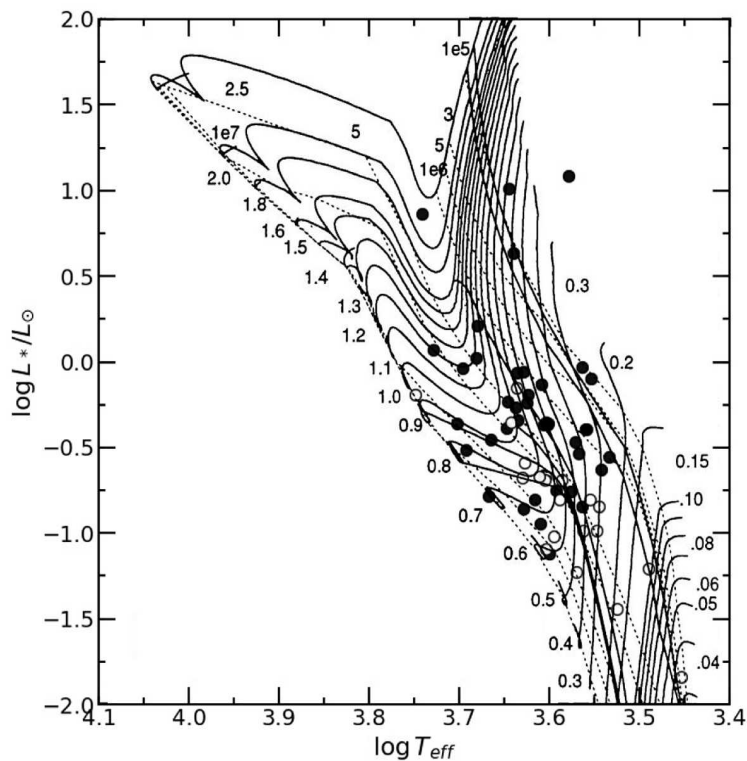


Fig. 1: HR diagram of the investigated PMS stars. The solid lines are Canuto & Mazzitelli [CM] Alexander evolutionary tracks (D’Antona & Mazzitelli 1994). The filled circle symbols and the open circles indicate PMS stars in molecular clouds and moving groups, respectively.

2 Observations

The observations were conducted with the Medium And Low Long slit Spectrograph (MALLS) mounted on the 2.0 m Nayuta Telescope at the Nishi-Harima Astronomical Observatory (NHAO), Japan. The data for four PMS stars was obtained between 2017 December 5 and 2019 February 6 with the 0.8'' width slit or the 1.2'' width slit using the $18001 \cdot \text{mm}^{-1}$ grating. These instrument settings achieved a wavelength coverage between 8350 \AA and 9360 \AA and a spectral resolution is between 7500 and 9000. The integration time for each object was between 600 s and 1200 s.

High-resolution spectroscopic observations of five PMS stars were conducted on September 18, 2007 with the High Dispersion Spectrograph (HDS; Noguchi et al. 2002) mounted on the Subaru Telescope. The data was obtained using the StdNIRb mode and with the 0.6'' width slit. These instrument settings achieved a wavelength coverage between 6650 Å and 9360 Å and a spectral resolution of 60,000. The integration time for each object was between 600 s and 1500 s.

Archive data of 26 PMS stars and 5 standard stars obtained with HIRES mounted on the Keck Telescope was also used. The observer, date of the observations, wavelength coverage, and integration times are listed in Table 2. The spectral resolution was 70,000. The archive data of six PMS stars obtained with the UVES ($R \sim 40,000$) mounted on the Very Large Telescope (VLT) was also used. The program IDs, principal investigators, and dates of the observations are listed in Table 2. The wavelength coverage was between 5655 Å and 9496 Å. The integration time for each object was between 10 s and 600 s. In addition, the archive data of 19 PMS stars obtained with the X-Shooter ($R \sim 8,000$) mounted on the VLT was also used. The wavelength coverage was between 5337 Å and 10200 Å. The integration time for each object was between 2 s and 600 s.

3 Data Reduction

The Image Reduction and Analysis Facility (IRAF) software package¹ was used for data reduction. Overscan subtraction, dark subtraction, flat fielding, wavelength calibration using an Fe-Ne-Ar lamp, removal of scattered light, extraction of a spectrum, and continuum normalization were conducted for all the spectra obtained by MALLS.

The HDS data was reduced with overscan subtraction, bias subtraction, flat fielding, removal of scattered light, extraction of a spectrum, wavelength calibration using a Th-Ar lamp, and continuum normalization. A detailed description of the data reduction methods used herein is presented in Takagi et al. (2015). The HIRES data was reduced with the Mauna Kea Echelle Extraction (MAKEE) package. The UVES data and X-Shooter data had already been reduced.

All object spectra were shifted to match the rest radial velocity. Therefore we measured the wavelengths of 2 un-blended Fe I absorption lines ($\lambda 8468.404, 8621.598$ Å), then shifted the wavelength of all spectra by the average of the difference between the measured wavelengths and laboratory wavelength.

The Ca II IRT emission lines are often located on the broad photospheric absorption lines of Ca II. In general, the photospheric absorption of the Ca II IRT line is strong, especially for K

¹ IRAF is distributed by the National Optical Astronomy Observatories, which are operated by the Association of Universities for Research in Astronomy, Inc., under cooperative agreement with the National Science Foundation.

type stars. And investigated PMS stars have late spectral type. An absorption line profile of a PMS spectrum could be obscured by continuum veiling. The amount of veiling, V , is defined as

$$V = \frac{W^0}{W} - 1, \quad (1)$$

where W^0 denotes the unveiled EQW and W is the veiled EQW.

In this study, inactive stars with a spectral type similar to that of the target object were used as template stars (the inactive stars library, Yee, Petigura & von Braun 2017 ; Passegger et al. 2018). We obtained the Keck archive data of five inactive stars, named ι Psc (F7), 16 Cyg (G3), HD 166 (G8), HD 88230 (K6), and GJ 412a (M1). For the correction of the rotational broadening, the spectra of the template stars were convolved with a Gaussian kernel to match the width of the absorption lines of each object. To estimate the amount of veiling, we measured the EQWs of Ti I, Fe I, and Cr I photospheric absorption lines between 8420 and 8700 Å (Table 3). In Table 3, absorption lines of several stars could not be measured because of varying wavelength ranges of the individual data archives. If the amount of the veiling was estimated for more than five absorption lines, we calculated their mean values and residuals. Basri & Batalha (1990) claimed that the veiling is constant around 8500 Å. We assumed that each of the Ca II IRT emission line has the same veiling value as all the others. We substituted the EQW of the lines of the PMS spectrum for W , that of the template star for W^0 , and then obtained the amount of veiling for each absorption line. The average value of V and standard deviation σ_V were calculated (Table 4). In case $V - \sigma$ is negative or the veiling values were measured for less than five absorption lines, we regarded V as 0.

For objects indicating a significant veiling value, we made a veiled spectrum of the template star. First, we added the veiling value V to the normalized spectrum of the template star. Then, the continuum component was normalized again to unity by dividing by $(1 + V)$. The veiled spectrum of the template star was subtracted from that of the target star indicating a significant veiling value. For objects indicating $V = 0$, the spectrum of the template star which was not veiled was subtracted.

Figure 2 shows the procedures of the spectral subtraction of the Ca II IRT lines of AA Tau. The solid line at the top of the panel shows the observed spectrum of AA Tau before subtraction of the spectrum of the template star. In this case, the Ca II IRT lines display emission profiles over a broad absorption feature. The dotted line is the fitted spectrum of the veiled template star. Continuum components of both spectra were normalized to unity. The solid line in the bottom of the panel represents the observed spectrum of AA Tau after subtracting the spectrum of the template star. Any broad absorption feature was removed completely, and only the emission component remained. Unfortunately, any absorption lines (Table 3) to measure the veiling value are not shown in Figure 2. The spectra of most objects only contain emission components after this subtraction has been performed. The sub-

traction of the template spectrum is necessary for a correct measurement of the EQWs for the Ca II IRT emission lines.

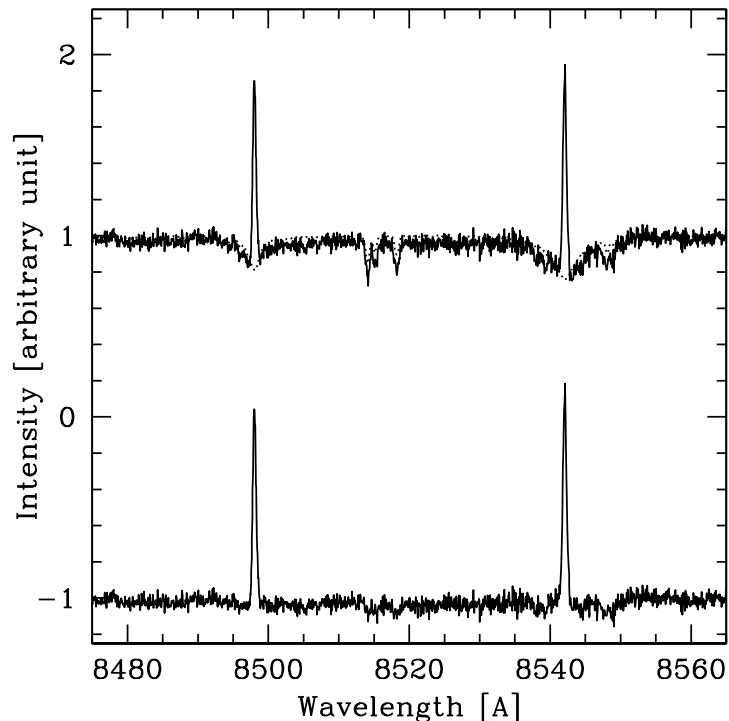


Fig. 2: The emission profiles of the Ca II IRT lines ($\lambda 8498, 8542 \text{ \AA}$). The observed spectrum of AA Tau is shown in the top of the panel with a solid line. The dotted line is the fitted inactive star, a K6 template star. The difference between the observed and template spectra is shown in the bottom of the panel, where the Ca II IRT narrow lines appear in the emission. The difference between the AA Tau spectrum and the template star’s spectrum is shown shifted by -1.0 for display purposes. Note that all of the nine absorption lines used for estimating the amount of the veiling (Table 3) are out of range for this figure.

Before measuring the EQWs, the continuum component of the spectra was added to unity. To obtain the EQWs of the Ca II IRT emission lines, the area of the emission profile was directly integrated. We also measured their full width at half maximums (FWHMs) by fitting with a Gaussian function. The EQW errors were estimated by multiplying the standard deviation of the continuum by the wavelength range of the emission line. The wavelength range for measuring standard deviation is $\lambda 8483 - 8492 \text{ \AA}$ for the Ca II $\lambda 8498, 8542 \text{ \AA}$ lines and $\lambda 8623 - 8632 \text{ \AA}$ for the Ca II $\lambda 8662$ line. These ranges are free from any emission and absorption lines. Further for our discussion we only consider emission profiles the S/N larger than 3, for calculating EQWs, FWHMs, etc.

Table 1: Physical parameters of the PMS stars.

Object Name	i	$(B-V)_0$	A_V	L/L_\odot	T_{eff}	dist	$v \sin i$	τ_c	$\log \dot{M}$	M_*	M_{conv}	Age	Tel.
(1)	mag	mag	mag	(5)	K	pc	$\text{km} \cdot \text{s}^{-1}$	$\times 10^6 \text{s}$	$M_\odot \cdot \text{yr}^{-1}$	M_\odot	M_\odot	Myr	(14)
Taurus-Auriga molecular cloud													
AA Tau	12.7	0.82	0.74	0.74	4060	136	12.7	20	-8.48	0.5	0.0	1.0	V
BP Tau	11.0	1.01	0.34	0.46	4320	128	10.9	14	-7.54	0.9	0.2	5.0	V
CX Tau	11.9	1.31	0.80	0.28	3417	127	19.1	19	-8.97	0.3	0.0	1.0	K
CoKu Tau4	12.6	1.30	1.75	0.11	4070	170	25.8	11	-10.0	0.6	0.2	20.0	K
DF Tau	10.4	0.75	0.45	0.93	3665	124	18.4	19	-7.62	0.3	0.0	0.3	V
DG Tau	11.5	0.54	1.30	0.34	3731	120	21.7	19	-6.30	0.4	0.0	1.0	N
DL Tau	11.6	0.53	2.00	0.44	3998	158	19.0	21	-6.79	0.6	0.0	2.0	N
DM Tau	12.6	0.82	1.10	0.18	3769	144	10.0	22	-7.95	0.5	0.0	5.0	K
DR Tau	10.8	0.46	0.61	0.86	4327	194	10.0	21	-6.50	0.7	0.0	1.0	V
DS Tau	11.3	0.78	0.34	0.43	4040	158	11.2	21	-7.89	0.6	0.0	2.0	K
FN Tau	11.8	1.27	1.40	0.14	4250	130	6.4	7	-	0.7	0.5	30.0	K
FP Tau	12.0	1.55	0.20	0.24	3486	128	27.9	19	-9.45	0.3	0.0	1.0	K
GH Tau	11.5	1.41	0.40	0.79	3580	140	25.2	19	-7.92	0.3	0.0	0.5	K
GM Aur	11.2	1.10	0.31	0.55	4338	158	12.6	14	-8.02	0.9	0.2	5.0	K
GO Tau	13.1	1.10	1.20	0.08	3984	143	19.2	4	-7.93	0.6	0.5	70.0	K
HBC 374	11.0	1.65	0.00	0.43	4007	125	12.9	21	-	0.6	0.0	2.0	S
HBC 376	11.4	1.08	0.00	0.28	4389	121	68.0	5	-8.92	0.8	0.6	30.0	S
HBC 407	11.9	1.03	0.00	0.16	4649	125	8.8	3	-	0.7	0.6	70.0	V
HBC 427	10.7	1.21	0.20	0.87	4249	148	10.0	21	-	0.7	0.0	1.0	K
HD 285778	9.7	0.72	0.23	1.18	5358	119	17.6	6	-8.03	1.3	1.0	7.0	S
HP Tau	-	1.55	0.39	0.29	3688	176	100.0	20	-8.47	0.4	0.0	2.0	V
IT Tau	12.5	1.18	3.10	0.18	3913	161	-	13	-	0.7	0.2	10.0	K
LkCa 04	11.3	1.38	0.35	0.40	3621	129	26.1	19	-8.73	0.4	0.0	1.0	K
LkCa 14	10.8	1.21	0.00	0.58	4218	127	21.9	22	-8.85	0.7	0.0	2.0	K
LkCa 15	11.0	1.08	0.60	0.64	4201	158	12.5	22	-8.87	0.7	0.0	2.0	K
LkCa 19	10.0	0.96	0.00	1.63	4784	158	19.8	16	-10.0	1.2	0.2	2.0	K
RY Tau ^(*)	9.3	0.86	1.50	6.30	5750	133	48.8	3	-7.11	1.8	1.7	5.0	N
SU Aur	8.9	0.58	0.90	4.31	4359	157	65.0	20	-8.25	0.6	0.0	0.2	V
UX Tau	10.0	0.92	0.36	0.59	4427	139	9.9	19	-9.00	0.9	0.1	3.0	K
V1023 Tau	11.0	1.24	1.35	0.43	4007	125	12.9	21	-7.78	0.6	0.0	2.0	N
V1204 Tau	10.1	0.88	0.31	1.05	4800	138	22.5	9	-	1.2	0.6	5.0	S
V1297 Tau	10.8	0.72	0.28	0.44	5039	117	17.5	2	-	0.9	0.9	50.0	K
V1321 Tau	12.0	1.35	0.70	0.22	4042	146	11.2	7	-	0.7	0.5	30.0	K
V1348 Tau	11.3	1.09	0.00	0.41	4441	155	4.8	12	-	0.9	0.3	7.0	K
V1840 Ori	11.1	0.97	0.20	0.59	4617	149	14.5	10	-	1.0	0.5	7.0	S
V830 Tau	11.1	1.22	0.30	0.44	4020	130	26.6	21	-8.10	0.6	0.0	2.0	K
V836 Tau	12.4	1.00	1.70	0.40	3631	168	13.4	19	-8.98	0.4	0.0	1.0	K
ZZ Tau	11.9	1.22	1.00	0.16	4130	134	21.4	7	-	0.7	0.5	30.0	K
Orionis OB 1c association													
HBC 167	10.4	0.70	0.00	7.32	5504	406	18.0	13	-	2.0	0.6	1.0	V
Upper Scorpius association													
1RXS J161951.4-215431	11.1	1.40	0.00	-	3746	-	-	2	-	-	-	-	K
Perseus molecular cloud													
LkH α 86	14.4	1.44	0.00	0.14	3657	321	6.8	20	-	0.4	0.0	5.0	K
LRL 72	-	2.24	0.00	0.51	3488	249	9.3	19	-	0.3	0.0	0.7	K
AB Doradus moving group													
HIP 17695	9.8	1.51	0.00	0.04	3349	16	18.0	19	-	0.2	0.0	20.0	V

Table 1: (Continued)

Object Name	i	$(B - V)_0$	A_V	L/L_\odot	T_{eff}	dist	$v \sin i$	τ_c	$\log \dot{M}$	M_*	M_{conv}	Age	Tel.
(1)	mag	mag	mag	(5)	K	pc	$\text{km} \cdot \text{s}^{-1}$	$\times 10^6 \text{s}$	$M_\odot \cdot \text{yr}^{-1}$	M_\odot	M_\odot	Myr	(14)
β Pictoris moving group													
HD 197481	7.4	1.46	0.04	0.10	3652	9	8.0	21	-	0.4	0.0	10.0	V
η Chamaeleontis cluster													
RECX 04	11.4	1.43	0.00	0.21	4023	99	6.0	13	-	0.7	0.2	10.0	V
RECX 06	12.4	1.42	0.00	0.10	3525	97	20.9	19	-	0.3	0.0	5.0	V
RECX 07	10.0	1.15	0.00	0.71	4325	98	30.0	22	-	0.8	0.0	3.0	V
RECX 09	12.8	1.46	0.00	0.10	3933	97	-	9	-10.4	0.6	0.3	30.0	V
RECX 10	11.3	1.42	0.00	0.21	4088	97	9.0	7	-	0.8	0.5	20.0	V
RECX 11	10.3	1.18	0.00	0.45	4392	98	13.0	12	-9.77	0.9	0.3	7.0	V
RECX 15	12.7	0.83	0.00	0.06	3719	91	28.0	11	-9.09	0.5	0.2	30.0	V
"Cha-Near" region													
RX J1147.7-7842	11.6	1.54	0.00	0.16	3881	106	-	9	-	0.7	0.4	20.0	V
RX J1204.6-7731	11.8	1.52	0.00	0.16	3584	100	6.0	20	-	0.4	0.0	3.0	V
TW Hydrae association													
TWA 01	10.0	0.89	0.27	0.26	4235	59	14.0	9	-8.74	0.9	0.5	10.0	V
TWA 06	10.3	1.23	0.27	0.21	4268	65	-	7	-	0.8	0.5	20.0	V
TWA 07	10.0	1.46	0.00	0.08	4017	33	4.4	9	-	0.6	0.3	30.0	V
TWA 14	11.3	1.27	0.10	0.20	3852	91	-	20	-	0.6	0.0	7.0	V
TWA 22	11.3	1.73	0.00	0.01	2843	19	9.7	2	-	0.0	0.0	0.7	V
TWA 23	10.6	1.50	0.05	0.14	3508	55	-	19	-	0.3	0.0	3.0	K
TWA 25	9.9	1.34	0.24	0.22	4019	53	12.9	7	-	0.8	0.5	20.0	V

(1) LRL 72 : Luhman et al. (2016) ; (2) i - mag : UCAC4 Catalogue (Zacharias et al. 2013) ; (3) $B - V$: van Leeuwen (2007), Mayne et al. (2007), Manoj et al. (2006), Henden et al. (2016), Herbig & Bell (1988), Hanson (2003), and Davies et al. (2014) ; (4) A_V : Kraus et al. (2009), Manoj et al. (2006), and Wahhaj et al. (2010), (5)(6) Luminosity and T_{eff} : *Gaia* DR2 (Gaia Collaboration 2018), Palla & Stahler (2002), Kenyon & Hartmann (1995), and Pecaut & Mamajek (2013) ; (7) Distance : *Gaia* DR2 (Bailer-Jones et al. 2018) ; (8) $v \sin i$: Glebocki & Gnacinski (2005), Nguyen et al. (2012), Torres et al. (2006), and Messina et al. (2011) ; (10) \dot{M} : Najita, Strom, & Muzerolle (2007), Gullbring et al. (1998), White & Ghez (2002), Hartmann et al. (1998), Lawson et al. (2004), Calvet et al. (2004), and Ingleby et al. (2013) (14) N : Nayuta Telescope ; S : Subaru Telescope ; K : Keck Telescope ; V : VLT (*) For RY Tau, A_V , L/L_\odot , T_{eff} , and the distance were taken from Garufi et al. (2019).

Table 2: Details of the archive data from Keck/HIRES, VLT/UVES, and VLT/X-Shooter

Program ID	PI-Observers	Observation Dates	Wavelength [\AA]	Integration Time [s]
Keck / HIRES				
C05H	N. Reid	1999-06-16	7600 - 9910	100
C77H	L. Hillenbrand	1999-12-06, 07	6240 - 8680	1200 - 1500
C109H	L. Hillenbrand	2000-01-10, 11	6240 - 8680	300 - 900
C240Hr	S. E. Dahm	2007-11-30	4880 - 9380	460 - 1800
C095Hr	S. E. Dahm	2008-12-03, 04	4450 - 8900	10 - 1200
N107Hr	I. Pascucci	2012-12-01	4880 - 9380	300 - 3710
C252Hr	L. Hillenbrand	2013-12-26, 27	4880 - 9380	150 - 600
C247Hr	J. Carpenter	2015-06-01, 02	4880 - 9380	305 - 424
C250Hr	L. Hillenbrand	2016-05-17	4880 - 9380	22
C226Hr	L. Hillenbrand	2017-01-13	4880 - 9380	130
VLT / UVES				
075.C-0321(A)	M. Hempel	2005-08-26	5655 - 9496	200
082.C-0005(B)	A. Scholz	2008-10-02, 2009-01-08, 18	5655 - 9496	10 - 600
VLT / X-Shooter				
084.C-1095(A)	G. Herczeg	2010-01-19, 2010-01-20	5337 - 10200	2 - 388
085.C-0238(A)	J. M. Alcalá	2010-04-06, 07	5337 - 10200	20 - 480
086.C-0173(A)	J. M. Alcalá	2010-01-12, 13	5337 - 10200	100 - 400
094.C-0327(A)	S. Alencar	2015-01-16	5337 - 10200	120
094.C-0805(A)	G. Herczeg	2015-01-15, 2015-03-07	5337 - 10200	24 - 600
094.C-0913(A)	C. F. Manara	2014-12-05	5337 - 10200	320 - 400

Table 3: Absorption lines for estimating the amount of veiling.

	Wavelength [\AA]
Ti I	8426.497
Ti I	8450.871
Cr I	8455.288
Fe I	8468.404
Fe I	8621.598
Fe I	8632.412
Ti I	8682.988
Fe I	8688.600
Ti I	8692.326

3 Results

The EQWs of the Ca II IRT emission lines and their errors are listed in Table 4. Seven objects have broad emission lines of Ca II $\lambda 8498 \text{ \AA}$ ($\text{FWHM} > 100 \text{ km} \cdot \text{s}^{-1}$), while most PMS stars exhibit narrow emission lines ($\text{FWHM} \leq 100 \text{ km} \cdot \text{s}^{-1}$). Figure 3 shows the spectra of the $\lambda 8498 \text{ \AA}$ emission line after subtracting the photospheric absorption. The emission lines of DG Tau, DL Tau, and DR Tau are broad and strong ($W_{\text{IRT}} \sim 50 \text{ \AA}$), while those of RY Tau, SU Aur, RECX 15, and RX J1147.7-7842 are broad but not strong ($W_{\text{IRT}} < 10 \text{ \AA}$). All EQWs of narrow emission lines are weaker than 5 \AA . We note that a part of the narrow emission component of the PMS stars could be buried by the photospheric absorption before removal. In our sample, most objects that belong to the moving group only have absorption lines before removal of the photospheric absorption.

We obtained the amount of the veiling for 27 objects. Among them the amount of veiling was measured in the previous studies for 13 objects. The correlation coefficient between the literature values and our measured values is 0.84. The literature value was found to be within the uncertainty of the measured V for 8 objects. We note that on multiple occasions the variation of the veiling value have often been reported in several literature (Basri & Batalha 1990; Batalha et al. 1996; Hartigan et al. 1989, 1991).

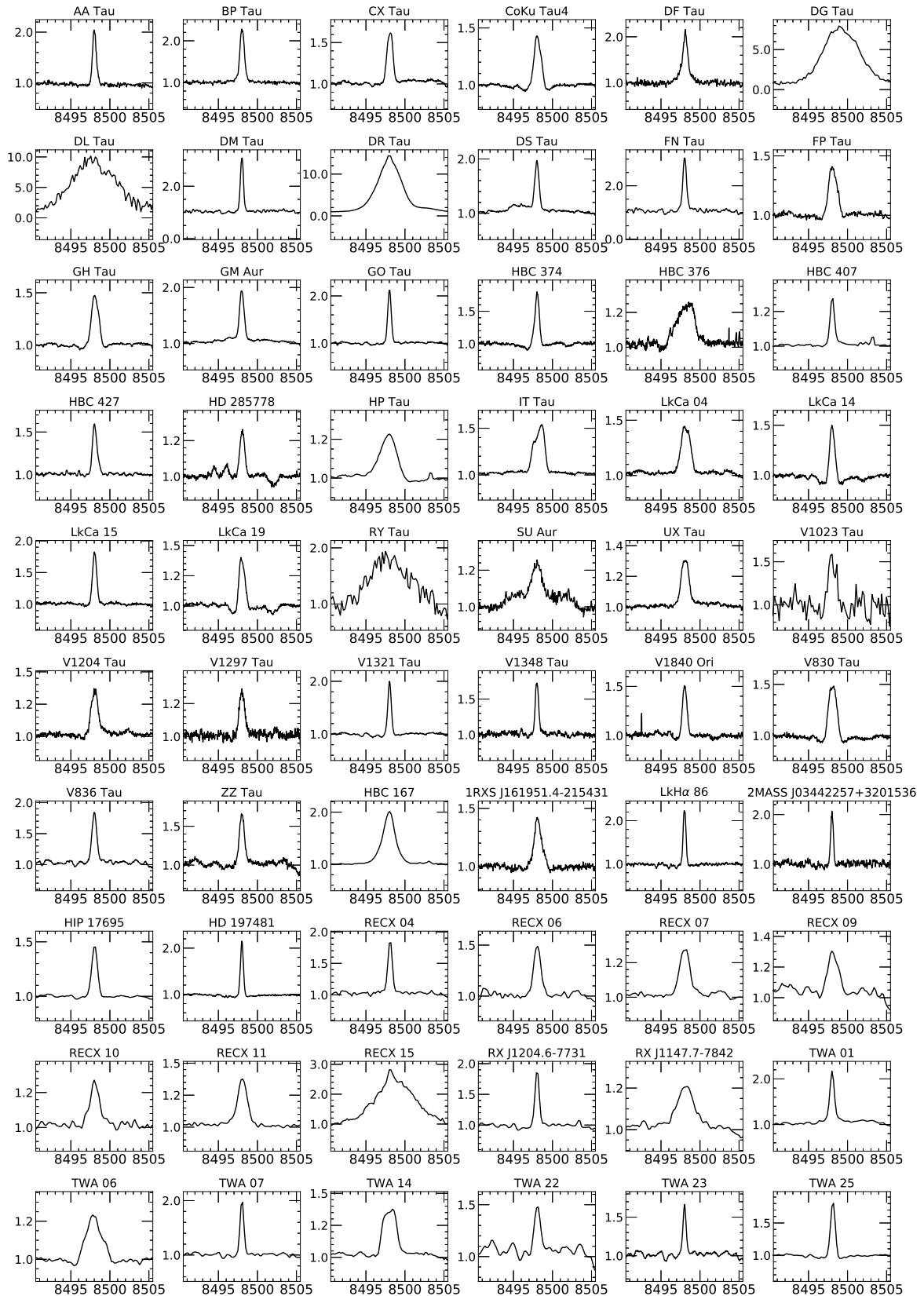


Fig. 3: Ca II IRT emission lines ($\lambda 8498 \text{ \AA}$) of all the PMS stars. The spectra are normalized to unity. Photospheric absorption lines have already been subtracted.

Table 4: EQWs, FWHMs of the Ca II IRT emission lines (λ 8498, 8542, 8662 Å) and the veiling value.

Object	$W_{\text{IRT}} [\text{Å}]$			FWHM [$\text{km} \cdot \text{s}^{-1}$]			Veiling
	$\lambda 8498$	$\lambda 8542$	$\lambda 8662$	$\lambda 8498$	$\lambda 8542$	$\lambda 8662$	
Taurus-Auriga molecular cloud							
AA Tau	0.65 ± 0.04	0.77 ± 0.04	0.61 ± 0.04	20	23	20	1.29 ± 1.20
BP Tau	1.05 ± 0.07	1.68 ± 0.12	1.15 ± 0.11	24	32	26	0.56 ± 0.40
CX Tau	0.59 ± 0.03	0.77 ± 0.04	0.72 ± 0.05	31	35	36	-0.11 ± 0.20
CoKu Tau4	0.53 ± 0.03	0.83 ± 0.04	0.60 ± 0.04	37	42	38	-
DF Tau	1.14 ± 0.15	2.02 ± 0.25	1.38 ± 0.19	33	55	45	-
DG Tau	49.49 ± 1.58	46.83 ± 1.74	51.39 ± 2.50	185	221	211	-
DL Tau	53.88 ± 8.14	50.65 ± 9.21	39.37 ± 7.89	249	271	250	-
DM Tau	1.02 ± 0.06	1.29 ± 0.09	1.07 ± 0.09	16	22	19	-0.19 ± 0.18
DR Tau	53.1 ± 0.73	59.83 ± 0.75	49.03 ± 0.30	126	163	153	2.64 ± 1.48
DS Tau	0.75 ± 0.04	1.19 ± 0.06	1.05 ± 0.04	26	35	35	0.35 ± 0.32
FN Tau	1.32 ± 0.10	-	1.49 ± 0.14	20	-	28	-0.18 ± 0.29
FP Tau	0.55 ± 0.04	-	0.55 ± 0.06	45	-	41	-
GH Tau	0.62 ± 0.04	0.72 ± 0.04	0.56 ± 0.03	38	40	37	-
GM Aur	0.73 ± 0.02	1.41 ± 0.02	1.15 ± 0.02	27	42	38	0.31 ± 0.16
GO Tau	0.62 ± 0.04	0.86 ± 0.05	0.72 ± 0.05	19	23	22	-0.20 ± 0.16
HBC 374	0.57 ± 0.03	0.97 ± 0.06	-	23	33	-	-
HBC 376	0.67 ± 0.08	0.90 ± 0.08	-	95	111	-	-
HBC 407	0.26 ± 0.01	0.33 ± 0.01	0.27 ± 0.01	24	27	25	-
HBC 427	0.44 ± 0.02	0.58 ± 0.03	0.52 ± 0.04	25	32	31	0.07 ± 0.17
HD 285778	0.24 ± 0.02	0.39 ± 0.04	-	26	41	-	-
HP Tau	0.56 ± 0.04	0.84 ± 0.05	0.72 ± 0.03	84	110	90	-
IT Tau	0.81 ± 0.03	1.05 ± 0.03	0.88 ± 0.06	55	61	58	0.12 ± 0.23
LkCa 04	0.62 ± 0.05	0.92 ± 0.06	0.83 ± 0.07	51	68	67	-
LkCa 14	0.54 ± 0.04	0.74 ± 0.04	0.62 ± 0.04	29	32	29	-
LkCa 15	0.56 ± 0.02	0.58 ± 0.02	0.56 ± 0.05	22	26	23	0.25 ± 0.17
LkCa 19	0.37 ± 0.02	0.51 ± 0.03	0.38 ± 0.03	32	36	31	0.40 ± 0.18
RY Tau	6.53 ± 1.57	4.94 ± 1.47	4.21 ± 1.17	222	220	170	-
SU Aur	1.11 ± 0.16	1.87 ± 0.19	1.51 ± 0.26	117	179	113	-
UX Tau	0.37 ± 0.02	0.49 ± 0.02	0.43 ± 0.03	40	41	45	-
V1023 Tau	0.88 ± 0.24	1.32 ± 0.29	-	43	53	-	-
V1204 Tau	0.37 ± 0.04	0.39 ± 0.03	-	35	36	-	-
V1297 Tau	0.30 ± 0.04	0.36 ± 0.04	0.28 ± 0.05	29	30	28	-
V1321 Tau	0.54 ± 0.02	0.73 ± 0.04	0.62 ± 0.04	19	24	22	-0.32 ± 0.16
V1348 Tau	0.40 ± 0.04	0.54 ± 0.05	0.42 ± 0.05	18	25	20	0.31 ± 0.33
V830 Tau	0.75 ± 0.04	1.17 ± 0.06	0.79 ± 0.04	43	46	40	-0.37 ± 0.14
V836 Tau	0.68 ± 0.05	0.84 ± 0.05	0.81 ± 0.06	28	40	34	0.08 ± 0.35

Table 4: (Continued)

Object	$W_{\text{IRT}} [\text{\AA}]$			FWHM [$\text{km} \cdot \text{s}^{-1}$]			Veiling
	$\lambda 8498$	$\lambda 8542$	$\lambda 8662$	$\lambda 8498$	$\lambda 8542$	$\lambda 8662$	
ZZ Tau	0.62 ± 0.07	0.84 ± 0.07	0.56 ± 0.08	28	33	35	-
Orionis OB 1c association							
HBC 167	1.93 ± 0.05	3.28 ± 0.08	2.43 ± 0.05	67	85	80	0.13 ± 0.26
Upper Scorpius association							
1RXS 215431	J161951.4- 0.55 ± 0.06	0.84 ± 0.07	0.69 ± 0.06	43	52	43	-
Perseus molecular cloud							
LkH α 86	0.62 ± 0.04	0.85 ± 0.06	0.68 ± 0.06	15	20	18	-0.24 ± 0.18
LRL 72	0.47 ± 0.04	0.58 ± 0.08	0.44 ± 0.07	15	20	21	-0.21 ± 0.19
AB Doradus moving group							
HIP 17695	0.42 ± 0.03	0.58 ± 0.06	0.41 ± 0.07	29	33	32	-
β Pictoris moving group							
HD 197481	0.57 ± 0.02	0.69 ± 0.03	0.56 ± 0.03	15	19	18	-
η Chamaeleontis cluster							
RECX 04	0.61 ± 0.07	0.84 ± 0.11	0.63 ± 0.08	23	31	25	0.08 ± 0.38
RECX 06	0.59 ± 0.08	0.71 ± 0.12	0.51 ± 0.10	38	43	40	-
RECX 07	0.58 ± 0.05	0.83 ± 0.07	0.67 ± 0.04	54	58	59	-
RECX 09	0.49 ± 0.11	0.92 ± 0.15	0.66 ± 0.11	57	85	78	-
RECX 10	0.52 ± 0.08	0.67 ± 0.09	0.51 ± 0.07	54	62	52	0.02 ± 0.21
RECX 11	0.59 ± 0.03	0.87 ± 0.05	0.72 ± 0.05	52	63	61	0.41 ± 0.83
RECX 15	9.28 ± 0.58	9.46 ± 0.58	7.32 ± 0.52	204	226	222	0.11 ± 0.40
"Cha-Near" region							
RX J1147.7-7842	0.57 ± 0.08	0.94 ± 0.09	0.63 ± 0.05	104	112	94	-
RX J1204.6-7731	0.64 ± 0.05	0.87 ± 0.07	0.64 ± 0.05	21	27	22	-
TW Hydrae association							
TWA 01	1.03 ± 0.07	1.96 ± 0.08	1.72 ± 0.10	26	38	35	0.37 ± 0.55
TWA 06	0.56 ± 0.03	0.90 ± 0.04	0.72 ± 0.05	80	85	83	-
TWA 07	0.62 ± 0.04	0.73 ± 0.05	0.55 ± 0.06	19	24	20	-
TWA 14	0.75 ± 0.05	1.15 ± 0.07	0.85 ± 0.07	66	81	76	0.03 ± 0.33
TWA 22	0.55 ± 0.12	1.06 ± 0.18	0.80 ± 0.18	32	56	74	-
TWA 23	0.36 ± 0.04	0.48 ± 0.06	0.29 ± 0.04	18	22	19	-0.22 ± 0.19
TWA 25	0.62 ± 0.02	0.82 ± 0.03	0.72 ± 0.03	24	27	26	-

4 Discussion

1 Emission Line Ratios of the Ca II IRT Lines

The ratios of the EQWs, $W_{\lambda 8542}/W_{\lambda 8498}$ and $W_{\lambda 8662}/W_{\lambda 8498}$ are sensitive to the conditions of the emitting plasma. It was shown that solar chromospheric plages and flares have the ratio of $1 \leq W_{\lambda 8542}/W_{\lambda 8498} \leq 2$ (Herbig & Soderblom 1980). In contrast, optically thin emission sources, such as solar prominences have a high value of this ratio, $W_{\lambda 8542}/W_{\lambda 8498} > 4$. In several studies (Herbig & Soderblom 1980 ; Hamann & Persson 1992a), TTSS showed small line ratios of the Ca II IRT emission lines, indicating dense chromospheric region such as plages and flares.

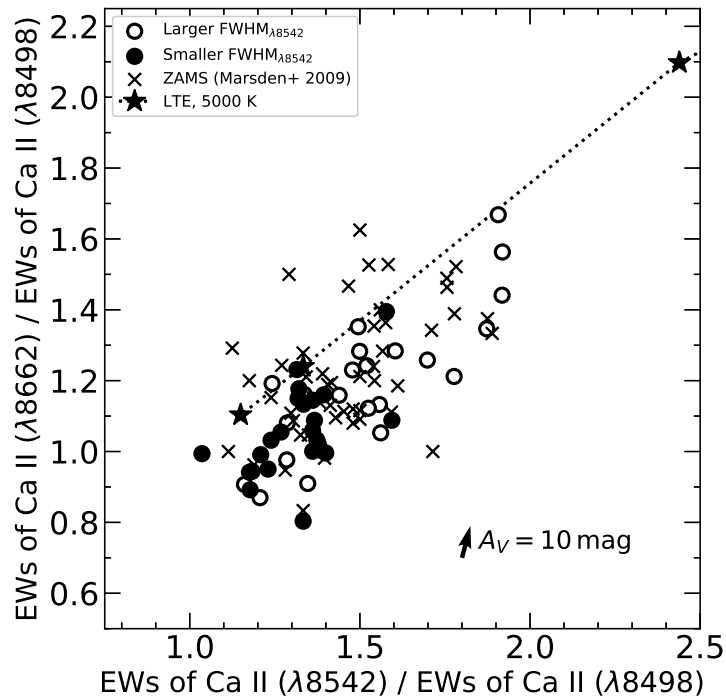


Fig. 4: Ratios of the EQWs of the Ca II IRT emission lines. The circle symbols represent the PMS stars in the molecular clouds and moving groups. The PMS stars are separated into two groups by the median of their $\text{FWHM}_{\lambda 8542}$; the open circles show the group of the PMS stars with a broader $\text{FWHM}_{\lambda 8542}$ than the median. The filled circles represent the narrower group. The low-mass stars in the young open clusters IC 2391 and IC 2602 are plotted as cross symbols (Marsden, Carter, & Donati 2009). The dotted line represents isothermal slabs ($T = 5000 \text{ K}$) in LTE (Herbig & Soderblom 1980 ; Hamann & Persson 1992a). The black star symbols on the line correspond to slab optical depths of 10, 100, and 1000, beginning from the upper right. The arrow in the lower right is the redding vector with $A_V = 10 \text{ mag}$.

The ratios of the EQWs of the Ca II IRT emission lines are plotted in Figure 4. The circle

symbols represent the PMS stars in the molecular clouds and the moving groups. The PMS stars are separated into two groups by the median of their $\text{FWHM}_{\lambda 8542}$; the open circles represent the group of the PMS stars with a broader $\text{FWHM}_{\lambda 8542}$ than the median. The filled circles represent the narrower group. For comparison, we also plotted the low-mass stars in the young open clusters IC 2391 and IC 2602 studied in Marsden, Carter, & Donati (2009) using cross symbols. The dotted line indicates isothermal slabs ($T = 5000$ K) in LTE (Herbig & Soderblom 1980 ; Hamann & Persson 1992a). The black star symbols on the line correspond to the slab optical depth of 10, 100, and 1000. The arrow in the lower right is the redding vector calculated by the equation below (Tokunaga 2000) with $A_V = 10$ mag,

$$\frac{A_\lambda}{A_V} = 0.41 \times (\lambda[\mu m])^{-1.75}. \quad (2)$$

As shown in Figure 4, the values of $W_{\lambda 8542}/W_{\lambda 8498}$ are 1.0 - 2.0 and $W_{\lambda 8662}/W_{\lambda 8498}$ are 0.7 - 1.7 for both, the PMS samples and cluster members. This suggests that the emission originates from the regions such as chromospheric plages and flares. Moreover, there is a tendency that emission lines showing relatively large $W_{\lambda 8542}/W_{\lambda 8498}$ are broad. The large FWHM of the line suggests a large turbulent velocity (Hamann & Persson 1992a).

Our results for the PMS stars are consistent with Herbig & Soderblom (1980), Hamann & Persson (1992a), and Frasca et al. (2017). Frasca et al. (2017) investigated the ratio of the line flux, $F_{\lambda 8542}/F_{\lambda 8498}$, of Class II and Class III objects in the Lupus star forming region. These objects have a low ratio of $1 < F_{\lambda 8542}/F_{\lambda 8498} < 2$. Not only the PMS stars in our sample but also the cluster members in IC 2391 and IC 2602 show a ratio of $W_{\lambda 8542}/W_{\lambda 8498}$ of 1.0 - 2.0, indicating that the Ca II IRT emission lines are emitted from the regions analogous to solar plages and flares.

The relationship between optical thickness and line broadening has been studied for the Ca II HK emission lines. Hamann & Persson (1989, 1992a) noticed that the Ca II HK emission lines of the TTSs are stronger and broader than the Ca II IRT emission lines. They interpreted that the Ca II HK emission lines are optically thicker than the Ca II IRT emission lines because the Ca II HK emission lines are generally stronger than the Ca II IRT emission lines. Cram & Giampapa (1987) calculated the Ca II K line profile in the non-LTE chromospheric model. According to this model, with a small chromospheric mass column density, the Ca II K line shows a narrow and weak emission. In case the mass column density increases, the Ca II K line exhibits not only stronger but also broader emissions. Batalha & Basri (1993) constructed photospheric and chromospheric models to match the Ca II HK and IRT emission line profiles of six PMS stars. They found that the lines are shaped by mass and temperature of the photosphere, the chromospheric temperature and microturbulence, and the temperature gradient of the lower chromosphere. A broad absorption line with a narrow emission

core at the line center was successfully reproduced in both CTTSs and WTTSs with the chromospheric models.

2 Chromospheric Activity and Mass Accretion Rate

We compared the strengths of the Ca II IRT emission lines and mass accretion rates to discuss whether the chromosphere is activated by mass accretion from the protoplanetary disk.

Mohanty, Jayawardhana, & Basri (2005) investigated the chromospheric activity of CTTSs, very low-mass young stars ($0.075 \leq M_* < 0.15 M_\odot$) and young brown dwarfs ($M_* \leq 0.075 M_\odot$). They selected "accretors" by applying a number of accretion diagnostics, such as an $H\alpha$ 10% width $\geq 200 \text{ km} \cdot \text{s}^{-1}$. For the accretors, the surface flux of the Ca II emission line, $F'_{\lambda 8662}$, showed a positive correlation with their mass accretion rate, \dot{M} , for approximately 4 orders of magnitude. Hence, they claim that the mass accretion rate can be estimated using the strength of the broad components of the Ca II IRT emission lines. In Mohanty, Jayawardhana, & Basri (2005), the mass accretion rates of CTTSs were taken from Muzerolle et al. (1998) and White & Basri (2003), in which the rates were estimated from the amount of the veiling in the U -, V - and R_C -bands. For the very low-mass young stars and the young brown dwarfs, the mass accretion rates were taken from Muzerolle et al. 2003, in which the rates were estimated from EQWs of the $H\alpha$ emission lines.

For calculating F'_{IRT} , a bolometric continuum flux per unit area at a stellar surface, F , was calculated at first. We used the i -band mag (the AB system) of the UCAC4 Catalogue (Zacharias et al. 2013), the stellar radius, and the distance of the objects (Table 1). F is given as

$$\log \frac{f}{f_0} = -\frac{2}{5} \times (m_{i^*} - A_I), \quad (3)$$

$$F = f \times \left(\frac{d}{R_*} \right)^2, \quad (4)$$

where f is the bolometric continuum flux of the object per unit area as observed on Earth. m_{i^*} is the apparent magnitude of the object in the i -band. The bolometric continuum flux per unit area under $m_i = 0 \text{ mag}$ (the AB system) condition, f_0 , is $1.852 \times 10^{-12} \text{ W} \cdot \text{m}^{-2} \cdot \text{A}^{-1}$ (Fukugita et al. 1996). A_I is the absorption coefficient for I mag, which is established with the absorption coefficient for V mag, A_V (van de Hurst 1968):

$$A_I = A_V \times 0.482. \quad (5)$$

d denotes the distance from an object to Earth (*Gaia* DR2: Bailer-Jones et al. 2018). Unfortunately, the distance from GH Tau is not listed in *Gaia* DR2, so we substituted that of the Taurus molecular cloud (140 pc). R_* is the stellar radius estimated using Stefan-Boltzmann's law with the photospheric

luminosity, T_{eff} , and the distance of the objects in *Gaia* DR2 (Gaia Collaboration 2018, Bailer-Jones et al. 2018). For object whose T_{eff} is not listed in *Gaia* DR2, we used the luminosity and T_{eff} listed in other papers: Palla & Stahler (2002) for AA Tau, Kenyon & Hartmann (1995) for GH Tau, Pecaut & Mamajek (2013) for HD 197481, RECX 09, and TWA 22. F was multiplied by the EQW of the Ca II IRT lines.

$$F'_{\text{IRT}} = F \times W_{\text{IRT}}, \quad (6)$$

F'_{IRT} are listed in Table 6. The relation between the mass accretion rate, \dot{M} , and the surface flux of the Ca II line, $F'_{\lambda 8662}$, is shown in Figure 5. \dot{M} listed in Table 1 were taken from several studies, in which the rates were estimated from the amount of veiling: Najita, Strom, & Muzerolle (2007) and Calvet et al. (2004) estimated \dot{M} with a continuum component between the visible and UV wavelengths, Gullbring et al. (1998), White & Ghez (2002), Hartmann et al. (1998), and Ingleby et al. (2013) determined \dot{M} from the amount of the continuum veiling in the *U*-band. For objects whose veiling had not been determined, we referred \dot{M} estimated with an EQW of the $H\alpha$ emission line (Lawson et al. 2004).

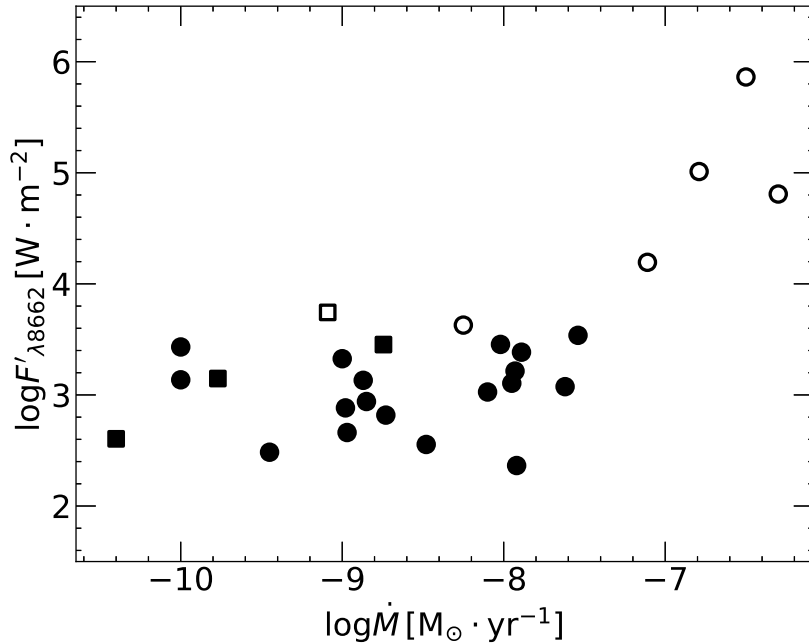


Fig. 5: Surface flux of the Ca II emission line, $F'_{\lambda 8662}$, as a function of mass accretion rate, \dot{M} . The circle symbols represent the PMS stars in the molecular clouds and the square symbols are the PMS stars in the moving groups. The open symbols show the objects with a broad Ca II IRT emission line ($\text{FWHM} > 100 \text{ km} \cdot \text{s}^{-1}$) and the filled symbols represent the objects with a narrow Ca II IRT emission line ($\text{FWHM} \leq 100 \text{ km} \cdot \text{s}^{-1}$).

In Figure 5, the circle symbols represent the PMS stars in the molecular clouds and the square

symbols are the PMS stars in the moving groups. The open symbols show objects with a broad Ca II IRT emission line ($\text{FWHM} > 100 \text{ km} \cdot \text{s}^{-1}$) and the filled symbols represent the objects with a narrow Ca II IRT emission line ($\text{FWHM} \leq 100 \text{ km} \cdot \text{s}^{-1}$). As mentioned above, the broad line components are well explained by the magnetospheric accretion model in Muzerolle et al. (1998), while the narrow emission Ca II lines are generated in the stellar chromosphere (Hamann & Persson 1992a).

We can see two groups among the PMS stars. High mass accretion rate PMS stars ($\dot{M} \gtrsim 10^{-7} M_{\odot} \cdot \text{yr}^{-1}$) have a broad Ca II IRT emission line. DG Tau, DL Tau, and DR Tau belong to this group. Those are classified as accretors based on the accretion diagnosis of Mohanty, Jayawardhana, & Basri (2005). The relationship between the mass accretion rate and the surface flux of the Ca II IRT emission line is consistent with that for the accretors (Mohanty, Jayawardhana, & Basri 2005). The mass accretion rate does not show any correlation with $F'_{\lambda 8662}$ for the objects with a narrow emission and almost all objects have $\log F'_{\lambda 8662} \sim 3$ with a flat distribution to \dot{M} . Those do not meet the accretor criteria presented by Mohanty, Jayawardhana, & Basri (2005). Most objects in our sample, including CTTSs, belong to this group. Any investigated PMS stars with a low mass accretion rate, except SU Aur and RECX 15, does not show broad Ca II IRT emission lines. The difference of F'_{IRT} between the two groups is more than 1 order of magnitude. We found that there is a significant difference between the group of the objects with a broad Ca II IRT emission line and the group of objects with a narrow Ca II IRT emission line. This has been well established difference between accretors and non-accretors by some studies, and our result supports that.

The Ca II IRT emission lines of PMS stars vary with time (e.g., JohnsKrull & Basri 1997). We present the EQWs and profiles of the Ca II IRT emission lines of BP Tau in Table 5. In this work, BP Tau shows narrow emissions superposed on broad absorption features. The $W_{\lambda 8662}$ of BP Tau in this study is 1.15 \AA . In contrast, the Ca II IRT lines in Mohanty, Jayawardhana, & Basri (2005) are broad and $W_{\lambda 8662}$ is 7.8 \AA . Mohanty, Jayawardhana, & Basri (2005) referred the EQWs of the Ca II IRT emission lines in Muzerolle et al. (1998), BP Tau as observed in 1996, has strong $F'_{\lambda 8662}$, similar to DG Tau, DL Tau and DR Tau. In Mohanty, Jayawardhana, & Basri (2005), objects with broad Ca II IRT emission lines as classified by Muzerolle et al. (1998) show a positive correlation with the mass accretion rate. Most objects in this study have narrow components, so that their $F'_{\lambda 8662}$ has no correlation with the mass accretion rate.

3 Rotation-Activity Relation

The narrow Ca II IRT emission lines in most of our samples are not correlated with the mass accretion rate. Noyes et al. (1984) used the Rossby number, N_R , as an indicator of stellar dynamo activity. We

Table 5: Time variation of the profiles of the CTTS, BP Tau

Observation Date	Profiles	$W_{\lambda 8662}$ [\AA]	Reference
1993	Narrow emission ($\lambda 8498$)	Not measured	Ardila et al. (2002)
1996	Broad emission + Narrow emission ($\lambda 8542$)	7.8	Muzerolle et al. (1998)
2006	Broad emission + Narrow emission ($\lambda 8498, 8542, 8662$)	6.44	Moto'oka & Itoh (2012)
2008	Narrow emission + Photospheric absorption ($\lambda 8498, 8542, 8662$)	1.15	This work

calculated N_R as follows,

$$N_R = \frac{2\pi R_*}{\tau_c v \sin i}, \quad (7)$$

where $v \sin i$ is taken from Catalog of Stellar Rotational Velocities (Glebocki & Gnacinski 2005), Nguyen et al. (2012), Torres et al. (2006), and Messina et al. (2011). For objects whose $v \sin i$ was not measured, we took the rotation period from Messina et al. (2010, 2011, 2018), Heinze et al. (2018), and the AAVSO International Variable Star Index (Watson et al. 2006). The rotation periods of IT Tau, TWA 06, TWA 14, TWA 23, and RECX 09 are 7.56 days, 0.54 days, 0.63 days, 1.03 days, and 1.71 days, respectively. R_* represents the stellar radius and τ_c is the convective turnover time.

We estimate τ_c of our PMS stars using pre-main sequence evolutionary tracks and convective turnover time of stars with $0.065 - 5.0 M_\odot$ presented in Jung & Kim (2007). The convective turnover time of a solar-mass PMS is between 300 and 100 days for the CTTS phase, and between a few hundred days and several dozens of days for the WTTS phase. The convective turnover time of an object near and on ZAMS remains stable at a few dozen days. In Jung & Kim (2007), the τ_c of low mass stars near the main sequence was not calculated. For objects whose τ_c was not calculated in Jung & Kim (2007), we apply the approximation from Noyes et al. (1984) when calculating τ_c with $(B - V)_0$. $(B - V)_0$ was calculated from $B - V$ (van Leeuwen 2007, Mayne et al. 2007, Manoj et al. 2006, Henden et al. 2016, Herbig & Bell 1988, Hanson 2003, and Davies et al. 2014) and A_V in Kraus et al. (2009), Manoj et al. (2006), and Wahhaj et al. (2010).

We calculated the ratio of the surface flux of the Ca II IRT lines to the stellar bolometric luminosity, R'_{IRT} , for each Ca II IRT line. R'_{IRT} is similar to the parameter R'_{HK} derived from the Ca II H and K lines, as described by Noyes et al. (1984). $R'_{\lambda 8542}$, the ratio of the surface flux of the $\lambda 8542 \text{ \AA}$ line to the stellar bolometric luminosity, has been previously used by Soderblom et al. (1993) and James & Jeffries (1997). In addition to $R'_{\lambda 8542}$, $R'_{\lambda 8498}$ and $R'_{\lambda 8662}$ were used by Marsden, Carter, & Donati (2009). In their study, $R'_{\lambda 8498}$ and $R'_{\lambda 8662}$ show qualitatively similar results to $R'_{\lambda 8542}$. R'_{IRT} involves $R'_{\lambda 8498}$, $R'_{\lambda 8542}$ and $R'_{\lambda 8662}$, which are determined individually for each of the Ca II IRT lines.

For calculating R'_{IRT} , F'_{IRT} are divided by σT_{eff}^4 .

$$R'_{\text{IRT}} = \frac{F'_{\text{IRT}}}{\sigma T_{\text{eff}}^4}, \quad (8)$$

where σ is Stefan-Boltzmann's constant. The dependence of the surface flux upon the T_{eff} of the objects is eliminated by this calculation. R'_{IRT} are listed in Table 6.

The chromospheric activity of ZAMS stars is considered to be induced by dynamo activity. Marsden, Carter, & Donati (2009) investigated the Ca II IRT emission lines of low-mass stars in the young open clusters, IC 2391 and IC 2602. For stars with $\log N_{\text{R}} \leq -1.1$, R'_{IRT} is constant at levels of $\log R'_{\lambda 8498} \sim -4.4$, $\log R'_{\lambda 8542} \sim -4.2$, and $\log R'_{\lambda 8662} \sim -4.3$. These regions are called the saturated regime. For stars with $\log N_{\text{R}} \geq -1.1$, R'_{IRT} decreases with increasing N_{R} . This region is called the unsaturated regime. Marsden, Carter, & Donati (2009) suggest that the chromosphere is completely filled by the emitting region for stars in the saturated regime.

Figure 6 shows R'_{IRT} as a function of N_{R} . The circle symbols represent PMS stars in molecular clouds and the square symbols are PMS stars in moving groups. The open circles and squares show objects with a broad Ca II IRT emission line and the filled circles and squares represent objects with a narrow Ca II IRT emission line. The cross symbols represent low-mass stars in IC 2391 and IC 2602, as studied in Marsden, Carter, & Donati (2009).

Most PMS stars have N_{R} and R'_{IRT} , which is similar to those of the cluster members in the saturated regime. We claim that the chromospheres of the PMS stars are activated by the magnetic field generated by the dynamo process and that the chromosphere of these stars are completely filled by the emitting region. It is consistent with the previous studies indicating that PMS stars have optically thick Ca II IRT emission lines (e. g. Batalha & Basri 1993; Hamann & Persson 1992a) and our result supports them. In contrast, three PMS stars with strong and broad emission lines (DG Tau, DL Tau and DR Tau) have a R'_{IRT} 2 orders of magnitude larger than the cluster members. We consider that strong emission lines are caused by heavy mass accretion from their protoplanetary disks.

Several researchers have pointed out that low-mass dwarfs showing strong Ca II emission lines also have strong X-ray emissions (Hodebine et al. 2017), strong magnetic fields (Linsky 2017; Valenti & Johns-Krull 2001), and that the flux variation of the Ca II lines is related to the coverage of their faculae or spots. Some of these features have already been found in low-mass PMS stars. Furthermore, it has to be investigated whether low-mass PMS stars have these other features.

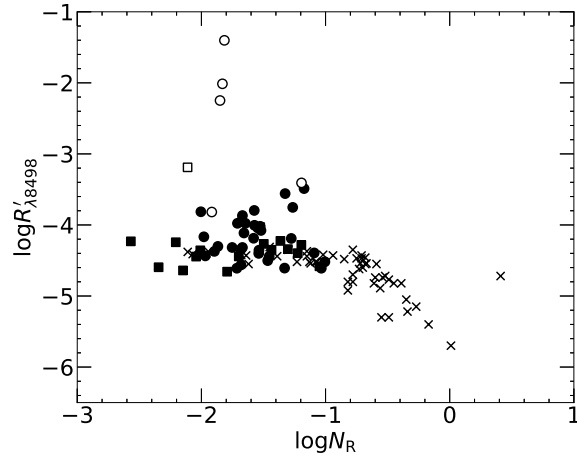
Table 6: F'_{IRT} , and R'_{IRT} of the Ca II IRT emission lines (λ 8498, 8542, 8662 \AA)

Object	$\log F'_{\lambda 8498}$ $\text{W} \cdot \text{m}^{-2}$	$\log F'_{\lambda 8542}$ $\text{W} \cdot \text{m}^{-2}$	$\log F'_{\lambda 8662}$ $\text{W} \cdot \text{m}^{-2}$	$\log R'_{\lambda 8498}$	$\log R'_{\lambda 8542}$	$\log R'_{\lambda 8662}$	$\log N_{\text{R}}$	note
	(1)	(2)	(3)	(4)	(5)	(6)	(7)	(8)
Taurus-Auriga molecular cloud								
AA Tau	2.58	2.65	2.55	-4.61	-4.54	-4.63	-1.71	NC
BP Tau	3.50	3.70	3.54	-3.80	-3.59	-3.76	-1.57	NC
CX Tau	2.57	2.69	2.66	-4.32	-4.20	-4.23	-1.75	NC
CoKu Tau4	3.38	3.57	3.43	-3.81	-3.62	-3.76	-2.00	NC
DF Tau	2.99	3.24	3.07	-4.02	-3.77	-3.94	-1.53	NC
DG Tau	4.79	4.77	4.81	-2.25	-2.27	-2.23	-1.85	BC
DL Tau	5.15	5.12	5.01	-2.01	-2.04	-2.15	-1.83	BC
DM Tau	3.08	3.19	3.11	-3.98	-3.87	-3.95	-1.71	NC
DR Tau	5.90	5.95	5.86	-1.40	-1.35	-1.44	-1.81	BC
DS Tau	3.24	3.44	3.38	-3.94	-3.74	-3.79	-1.68	NC
FN Tau	3.78	-	3.83	-3.49	-	-3.44	-1.17	NC
FP Tau	2.49	-	2.48	-4.44	-	-4.44	-1.97	NC
GH Tau	2.41	2.47	2.36	-4.56	-4.50	-4.61	-1.68	NC
GM Aur	3.26	3.54	3.45	-4.04	-3.76	-3.85	-1.55	NC
GO Tau	3.15	3.29	3.21	-4.00	-3.86	-3.94	-1.57	NC
HBC 374	2.85	3.08	-	-4.32	-4.08	-	-1.67	NC
HBC 376	3.50	3.63	-	-3.82	-3.69	-	-	NC
HBC 407	2.82	2.91	2.83	-4.61	-4.52	-4.60	-1.03	NC
HBC 427	2.83	2.95	2.90	-4.44	-4.32	-4.37	-1.45	NC
HD 285778	3.06	3.27	-	-4.61	-4.40	-	-1.33	NC
HP Tau	-	-	-	-	-	-	-2.54	NC
IT Tau	3.57	3.67	3.60	-3.56	-3.45	-3.52	-1.33	NC
LkCa 04	2.69	2.86	2.82	-4.30	-4.13	-4.17	-1.87	NC
LkCa 14	2.88	3.02	2.94	-4.37	-4.24	-4.31	-1.90	NC
LkCa 15	3.13	3.15	3.13	-4.11	-4.10	-4.12	-1.66	NC
LkCa 19	3.13	3.27	3.14	-4.34	-4.21	-4.34	-1.68	NC
RY Tau	4.38	4.26	4.19	-3.41	-3.53	-3.60	-1.19	BC
SU Aur	3.49	3.72	3.63	-3.82	-3.59	-3.68	-1.92	BC
UX Tau	3.26	3.39	3.33	-4.08	-3.95	-4.01	-1.52	NC
V1023 Tau	3.30	3.47	-	-3.87	-3.69	-	-1.67	NC
V1204 Tau	3.08	3.11	-	-4.40	-4.37	-	-1.54	NC
V1297 Tau	3.04	3.11	3.02	-4.52	-4.45	-4.55	-1.01	NC
V1321 Tau	2.99	3.12	3.04	-4.19	-4.06	-4.13	-1.28	NC
V1348 Tau	2.95	3.08	2.98	-4.39	-4.26	-4.37	-1.09	NC
V830 Tau	3.00	3.20	3.03	-4.17	-3.97	-4.14	-1.98	NC

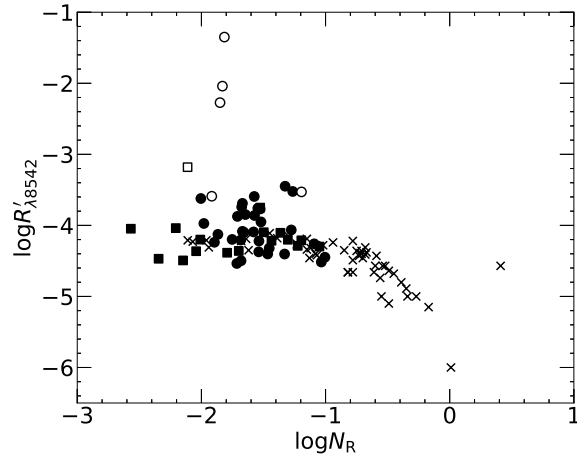
Table 6: (Continued)

Object	$\log F'_{\lambda 8498}$ $W \cdot m^{-2}$	$\log F'_{\lambda 8542}$ $W \cdot m^{-2}$	$\log F'_{\lambda 8662}$ $W \cdot m^{-2}$	$\log R'_{\lambda 8498}$	$\log R'_{\lambda 8542}$	$\log R'_{\lambda 8662}$	$\log N_R$	note
	(1)	(2)	(3)	(4)	(5)	(6)	(7)	(8)
V836 Tau	2.81	2.90	2.88	-4.19	-4.09	-4.11	-1.58	NC
ZZ Tau	3.24	3.37	3.20	-3.98	-3.85	-4.02	-1.65	NC
Orionis OB 1c association								
HBC 167	3.96	4.19	4.06	-3.75	-3.52	-3.65	-1.26	NC
Upper Scorpius association								
1RXS J161951.4-215431	-	-	-	-	-	-	-	NC
Perseus molecular cloud								
LkH α 86	2.65	2.79	2.69	-4.36	-4.22	-4.32	-1.54	NC
LRL 72	-	-	-	-	-	-	-1.32	NC
AB Doradus moving group								
HIP 17695	2.21	2.36	2.21	-4.64	-4.49	-4.64	-2.15	NM
β Pictoris moving group								
HD 197481	2.56	2.64	2.56	-4.44	-4.36	-4.45	-1.70	NM
η Chamaeleontis cluster								
RECX 04	2.83	2.97	2.85	-4.34	-4.20	-4.33	-1.30	NM
RECX 06	2.50	2.58	2.44	-4.44	-4.36	-4.51	-2.04	NM
RECX 07	2.94	3.10	3.00	-4.36	-4.20	-4.29	-2.01	NM
RECX 09	2.48	2.75	2.60	-4.66	-4.39	-4.53	-1.79	NM
RECX 10	2.80	2.91	2.79	-4.40	-4.29	-4.41	-1.22	NM
RECX 11	3.06	3.23	3.15	-4.27	-4.10	-4.18	-1.50	NM
RECX 15	3.85	3.85	3.74	-3.19	-3.18	-3.29	-2.11	BM
"Cha-Near" region								
RX J1147.7-7842	2.85	3.07	2.90	-4.26	-4.04	-4.21	-	BM
RX J1204.6-7731	2.62	2.76	2.62	-4.35	-4.22	-4.35	-1.44	NM
TW Hydrae association								
TWA 01	3.23	3.51	3.45	-4.03	-3.75	-3.81	-1.53	NM
TWA 06	3.03	3.24	3.14	-4.24	-4.04	-4.13	-2.21	NM
TWA 07	2.89	2.96	2.84	-4.28	-4.21	-4.33	-1.20	NM
TWA 14	2.87	3.05	2.92	-4.23	-4.05	-4.18	-2.57	NM
TWA 22	1.99	2.27	2.15	-4.58	-4.30	-4.42	-1.05	NM
TWA 23	2.34	2.46	2.24	-4.60	-4.47	-4.69	-2.34	NM
TWA 25	2.95	3.07	3.01	-4.22	-4.10	-4.16	-1.36	NM

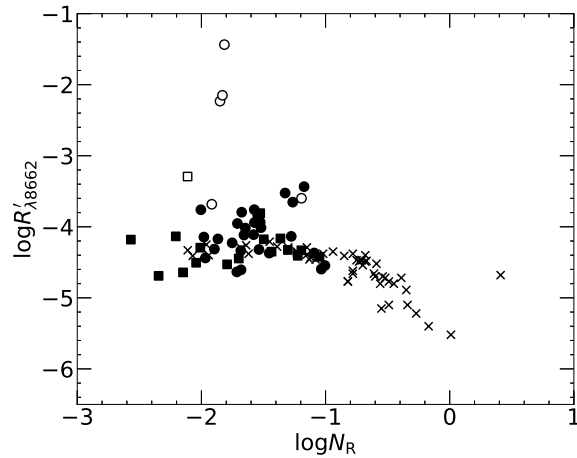
(8) This column shows the groups based on the FWHM of the Ca II emission lines ($\lambda 8498 \text{ \AA}$) and the membership of the objects. NC: Narrow emission objects belonging to the molecular clouds, BC: Broad emission objects belonging to the molecular clouds, NM: Narrow emission objects belonging to the moving groups, BM: Broad emission objects belonging to the moving groups



(a) CaII $\lambda 8498 \text{ \AA}$



(b) CaII $\lambda 8542 \text{ \AA}$



(c) CaII $\lambda 8662 \text{ \AA}$

Fig. 6: Relation between the ratio of the surface flux of the Ca II IRT line to the stellar bolometric luminosity, R'_{IRT} and the Rossby number, N_R . The circle symbols represent PMS stars in molecular clouds and the square symbols indicate PMS stars in moving groups. The filled symbols represent PMS stars with narrow Ca II IRT emission lines and the open symbols show PMS stars with broad Ca II IRT emission lines. The cross symbols represent low-mass stars in the young open clusters IC 2391 and IC 2602, as studied in Marsden, Carter, & Donati (2009).

5 Conclusion

In this paper, we investigated the Ca II infrared triplet lines ($\lambda 8498 \cdot 8542 \cdot 8662 \text{ \AA}$) of 60 PMS stars. The observations were conducted with Nayuta/MALLS and Subaru/HDS. Archived data obtained from the Keck/HIRES, VLT/UVES, and VLT/X-Shooter were also used.

1. The ratios of the equivalent widths of the Ca II IRT emission lines $W_{\lambda 8542}/W_{\lambda 8498}$ are 1.0–2.0 and $W_{\lambda 8662}/W_{\lambda 8498}$ are 0.7–1.7 for both PMS stars and the low-mass stars in the young open clusters (Marsden, Carter & Donati 2009). This suggests that the Ca II IRT emission lines originate from the regions analogous to solar plages and flares.
2. Seven PMS stars (DG Tau, DL Tau, DR Tau, RY Tau, SU Aur, RECX 15, and RX J1147.7-7842) have broad Ca II IRT emission lines. It is suggested that their broad emissions result from heavy mass accretion from their protoplanetary disks.
3. Most PMS stars have narrow Ca II IRT emission lines similar to low-mass stars in young open clusters. The emissions of these objects indicate no correlation with the mass accretion rate. The surface flux of the Ca II IRT emission lines to the stellar bolometric luminosity, R'_{IRT} , of these objects are large, as the largest R'_{IRT} of the cluster members. Most PMS stars have chromospheric activity similar to zero-age main-sequence stars. The chromosphere of these stars are completely filled by the Ca II emitting region.

Acknowledgments

This research has made use of the Keck Observatory Archive (KOA), which is operated by the W. M. Keck Observatory and NASA Exoplanet Science Institute (NExScI), and it is under contract with the National Aeronautics and Space Administration, and is based on the observations made with ESO Telescopes at the La Silla Paranal Observatory under programmes ID 075.C-0321, 082.C-0005, 084.C-1095, 085.C-0238, 086.C-0173, 094.C-0327, 094.C-0805, and 094.C-0913.

References

- Alencar, S. H. P., & Batalha, C. 2002, 378
- Ardila, D. R., Basri, G., Walter, F. M., Valenti, J. A., & Johns-Krull, C. M. 2002, *ApJ*, 567, 1013
- Bailer-Jones, C. A. L., Rybizki, J., Fousneau, M., Mantelet, G., & Andrae, R. 2018, *ApJ*, 156, 58
- Basri, G., & Batalha, C. 1990, *ApJ*, 363, 654
- Batalha, C. C., & Basri, G. 1993, *ApJ*, 412, 363.
- Batalha, C. C., Stout-Batalha, N. M., Basri, G., & Terra, M. A. O. 1996, *ApJS*, 103, 211.
- Bouvier, J. 1990, *ApJ*, 99, 946
- Calvet, N., Basri, G., & Kuhl, L. V. 1984, *ApJ*, 277, 725

Calvet, N., & Gullbring, E. 1998, *ApJ*, 509, 802

Calvet, N., Hartmann, L., Wilner, D., Walsh, A., & Sitko, M. L. 2004, in *Debris Disks and the Formation of Planets*, Vol. 324, 205

Cram, L. E., & Giampapa, M. S. 1987, *ApJ*, 323, 316

D'Antona, F., & Mazzitelli, I. 1994, *ApJS*, 90, 467

Davies, A. G., Veeder, G. J., Hill, S. I., Matson, D. L., & Johnson, T. V. 2014, *Icarus*, 241, 190

Frasca, A., Biazzo, K., Alcalá, J. M., et al. 2017, *A&A*, 602, 33

Fukugita, M., Ichikawa, T., Gunn, J. E., et al. 1996, *ApJ*, 111, 1748

Gaia Collaboration, 2018, *A&A*, 616, 1

Garufi, A., Podio, L., Bacciotti, F., et al. 2019, *A&A*, 628, 68

Ghez, A. M., Neugebauer, G., & Matthews, K. 1993, *ApJ*, 106, 2005

Glebocki, R., & Gnacinski, P. 2005, *VizieR Online Data Cat*, 3244

Glebocki, R., & Stawikowski, A. 2000, *ACA*, 50, 509

Gullbring, E., Hartmann, L., Bricen, C., & Calvet, N. 1998, *ApJ*, 429, 323

Hamann, F. W., & Persson, S. E. 1989, *ApJ*, 339, 1078

Hamann, F., & Persson, S. E. 1992a, *ApJS*, 82, 247

Hamann, F. W., & Persson, S. E. 1992b, *ApJS*, 82, 285

Hanson, M. M. 2003, *ApJ*, 597, 957

Hartigan, P., Hartmann, L., Kenyon, S., & Hewett, R. 1989, *ApJS*, 70, 899

Hartigan, P., Kenyon, S. J., Hartmann, L., et al. 1991, *ApJ*, 617

Hartmann, L. W., Stahler, S. W., & Mathieu, R. D. 1986, *ApJ*, 309, 275

Hartmann, L. W., Soderblom, D. R., & Stauffer, J. R. 1987, *AJ*, 93, 907

Hartmann, L. W., Calvet, N., Gullbring, E., & DAlessio, P. 1998, *ApJ*, 495, 385

Hartmann, L., Herczeg, G., & Calvet, N. 2016, *Annu Rev Astron Astrophys*, 54, 135

Heinze, A. N., Tonry, J. L., Denneau, L., et al. 2018, *ApJ*, 156, 241

Henden, A. A., Templeton, M., Terrell, D., et al. 2016, *VizieR Online Data Cat*, 2336

Herbig, G. H., & Bell, K. R. 1988, *LicOB*, 1111, 1

Herbig, G. H., & Soderblom, D. R. 1980, *ApJ*, 242, 628

Houdebine, E. R., Mullan, D. J., Bercu, B., Paletou, F., & Gebran, M. 2017, *ApJ*, 837, 96

Ingleby, L., Calvet, N., Herczeg, G., et al. 2013, *ApJ*, 767, 112

James, D. J., & Jeffries, R. D. 1997, *MNRAS*, 291, 252

JohnsKrull, C. M., & Basri, G. 1997, *ApJ*, 474, 433

Jung, Y. K., & Kim, Y.-C. 2007, *J. Astron. Space Sci.*, 25, 1

Katsukawa, Y., Berger, T. E., Ichimoto, K., et al. 2007, *Science*, 318, 1594

Kenyon, S. J., & Hartmann, L. 1995, *ApJ*, 101, 117

Kim, S.-L., Cha, S.-M., Lim, B., et al. 2016, *J Korean Astron Soc*, 49, 199

Kraus, A. L., Ireland, M. J., Hillenbrand, L. A., & Martinache, F. 2012, *ApJ*, 745, 19

Kraus, S., Hofmann, K.-H., Malbet, F., et al. 2009, *A&A*, 508, 787

Lawson WA, Lyo AR, Muzerolle J. 2004. *MNRAS*. 351, 39

- Leinert, C., Zinnecker, H., Weitzel, N., et al. 1993, *A&A*, 278, 129
- Linsky, J. L. 2017, *Annu Rev Astron Astrophys*, 55, 159
- Livingston, W., Wallace, L., White, O. R., & Giampapa, M. S. 2007, *ApJ*, 657, 1137
- Luhman, K. L., Esplin, T. L., & Loutrel, N. P. 2016, *ApJ*, 827, 52
- Manoj, P., Bhatt, H. C., Maheswar, G., & Muneer, S. 2006, *ApJ*, 653, 657
- Marsden, S. C., Carter, B. D., & Donati, J. F. 2009, *MNRAS*, 399, 888
- Mayne, N. J., Naylor, T., Littlefair, S. P., Saunders, E. S., & Jeffries, R. D. 2007, *MNRAS*, 375, 1220
- Mellon, S. N., Mamajek, E. E., Oberst, T. E., & Pecaut, M. J. 2017, *ApJ*, 844, 66
- Messina, S., Desidera, S., Turatto, M., Lanzafame, A. C., & Guinan, E. F. 2010, *A&A*, 520, 15
- Messina, S., Desidera, S., Lanzafame, A. C., Turatto, M., & Guinan, E. F. 2011, *A&A*, 532, 10
- Mohanty, S., Jayawardhana, R., & Basri, G. 2005, *ApJ*, 626, 498
- Moto'oka, K., & Itoh, Y. 2012, *RAA*, 13, 1189
- Muzerolle, J., Hartmann, L., & Calvet, N. 1998, *ApJ*, 116, 455
- Muzerolle, J., Hillenbrand, L., Calvet, N., Briceo, C., & Hartmann, L. 2003, *ApJ*, 592, 266
- Najita, J. R., Strom, S. E., & Muzerolle, J. 2007, *MNRAS*, 378, 369
- Navascues, D. B. y, Stauffer, J. R., & Jayawardhana, R. 2004, *ApJ*, 614, 386
- Neuhauser, R., Strezik, M. F., Schmitt, J. H. M. M., Wichmann, R., & Krautter, J. 1995, *A&A*, 297, 391
- Nguyen, D. C., Brandeker, A., Kerkwijk, M. H. Van, et al. 2012, *ApJ*, 745, 119
- Noguchi, K., Aoki, W., Kawanomoto, S., et al. 2002, *PASJ*, 54, 855
- Noyes, R. W., Hamann, F. W., Baliunas, S. L., & Vaughan, A. H. 1984, *ApJ*, 279, 763
- Palla, F., & Stahler, S. W. 2002, *ApJ*, 581, 1194
- Parker, E. N. 1955, *ApJ*, 122, 293
- Passegger, V. M., Reiners, A., Jeffers, S. V, et al. 2018, *Astrophys A&A*, 615, 6
- Pecaut, M. J., & Mamajek, E. E. 2013, *ApJS*, 208, 9
- Skumanich, A. 1972, *ApJ*, 171, 565
- Soderblom, D. R., Stauffer, J. R., & Hudon, J. D. 1993, *ApJ*, 85, 315
- Stauffer, J. R., Hartmann, L. W., Prosser, C. F., et al. 1997, *ApJ*, 479, 776
- Takagi, Y., Itoh, Y., Oasa, Y., & Sugitani, K. 2011, *PASJ*, 63, 677
- Tokunaga, A. T. 2000, in *Allen's Astrophysical Quantities* ed. A. N. Cox (Springer, New York, NY), 158
- Torres, C. A. O., Quast, G. R., Da Silva, L., et al. 2006, *A&A*, 460, 695
- Valenti J. A., Johns-Krull C. 2001. In *Magnetic Fields Across the timeprung-Russell Diagram*, ed. G. Mathys, S. K. Solanki, D. T. Wickramasinghe. ASP Conf. Ser. 248:179. San Francisco: ASP
- van de Hurst, 1968, *Nebulae and Interstellar Matter*
- van Leeuwen, F. 2007, *A&A*, 474, 653
- Vernazza, J. E., Avrett, E. H., & Loeser, R. 1981, *ApJS*, 45, 635
- Vogel, S. N., & Kuhl, L. V. 1981, *ApJ*, 245, 960
- Wahhaj, Z., Cieza, L., Koerner, D. W., et al. 2010, *ApJ*, 724, 835
- Watson, C. L., Henden, A. A., & Price, A. 2006, *JAVSO*, 35, 318

Wilson, O. C. 1978, ApJ, 226, 379

White, R. J., & Basri, G. 2003, ApJ, 582, 1109

White, R. J., & Ghez, A. M. 2002, ApJ, 556, 265

Yee, S. W., Petigura, E. A., & von Braun, K. 2017, ApJ, 836, 77

Zacharias, N., Finch, C. T., Girard, T. M., et al. 2013, ApJ, 145, 1

Zuckerman, B., & Song, I. 2004, A&A, 42, 685